Published in final edited form as:
J Nanosci Nanotechnol. 2011 April ; 11(4): 3621–3629.

Deposition of Silver Nanoparticles on Dendrimer Functionalized Multiwalled Carbon Nanotubes: Synthesis, Characterization and Antimicrobial Activity

Gururaj M. Neelgund and **Aderemi Oki***
Department of Chemistry, Prairie View A&M University, Prairie View, Texas 77446, USA

Abstract

The nanohybrids composed of silver nanoparticles and aromatic polyamide functionalized multiwalled carbon nanotubes (MWCNTs) is successfully synthesized and tested for their antibacterial activity against different pathogens. Prior to deposition of silver nanoparticles, acid treated MWCNTs (MWCNTs-COOH) were successively reacted with *p*-phenylenediamine and methylmethacrylate to form series of NH_2-terminated aromatic polyamide dendrimers on the surface of MWCNTs through Michael addition and amidation. Existence of high abundance of amine groups on the surface of functionalized MWCNTs (*f*-MWCNTs) provided sites for formation of silver nanoparticles by the reduction of aqueous solution of $AgNO_3$. The silver nanoparticles formed in the resulted *f*-MWCNTs-Ag nanohybrids were determined to be face centered cubic (fcc) symmetry. The structure and nature of *f*-MWCNTs and *f*-MWCNTs-Ag nanohybrids were characterized by UV-vis spectroscopy, Fourier transform infrared spectroscopy (FTIR), powder X-ray diffraction analysis (XRD), Raman spectroscopy and thermogravimetric analysis (TGA). The dispersion state of *f*-MWCNTs and immobilization of silver nanoparticles on the surface of *f*-MWCNTs were investigated by scanning electron microscopy (SEM) and transmission electron microscopy (TEM). Elemental composition of *f*-MWCNTs-Ag nanohybrids was determined by energy dispersive X-ray spectroscopy (EDS). The antimicrobial activity of *f*-MWCNTs-Ag nanohybrids were estimated against *E. coli, P. aeruginosa* and *S. aureu* and compared with MWCNTs-COOH and *f*-MWCNTs. The results indicate that functionalization of MWCNTs with aromatic polyamide dendrimers and successive deposition of Ag nanoparticles could play an important role in the enhancement of antimicrobial activity.

Keywords

Carbon Nanotubes; Silver Nanoparticles; Dendrimer; Antimicrobial Activity; Functionalization

1. INTRODUCTION

Recently, carbon nanotubes (CNTs) have attracted significant scientific interest ranging from nanoelectronics to biomedical applications owing to their unique structure and properties.1⁻5 Despite these great promises, many real applications of CNTs have been impeded by difficulties associated with their processing and manipulation. However, as produced CNTs have the tendency to exist in bundles rather than as individual tubes, because of strong van der Waals interactions, leading to insolubility in most organic media, and therefore limiting the range of applications. A common technique to improve dispersion

*Author to whom correspondence should be addressed. aroki@pvamu.edu.

and achieve optimum utilization of CNTs is through chemical functionalization, which enables chemical bonding between the CNTs and material of interest. Both covalent[6–10] and noncovalent[11–15] functionalization methods have been employed to impart solubility and chemical modifications to CNTs. Generally, the linkage of small or large molecules to CNTs by covalent methods is more stable and effective because grafted molecules raise the solubility of CNTs even with a low degree of functionalization.[16–19] One of the most common methods of covalently functionalizing CNTs employs reactions with carboxylic acid (–COOH) residues on CNTs, which are usually introduced by oxidation with strong acids at the more reactive (open) end or defect sites, instead of with their side walls.[20–22] This approach has been proven to be simple and does not require multiple organic synthesis steps. The carboxylic acid groups formed at the ends, and defect sites of CNTs, are commonly used for precursor functionalization in the formation of amine, ester and organometallic structures.[6, 23] Formation of amino-terminated nanotubes is a critical step in covalently linked nanotubes and biomolecules because amino groups act as chemical bridges. Among the various functionalizing molecules for CNTs, dendrimers are of particular interest as they have some unique properties because of their globular structure and tunable cavities.[24–26] The unique properties of dendrimers make them an ideal platform to covalently link dyes, targeting ligands, and drugs for multifunctional imaging, targeting, and therapeutic treatment of cancer cells.[27–29] Furthermore, through various templating, stabilization, or assembly approaches, dendrimer entrapped, dendrimer-stabilized, or dendrimer-assembled nanoparticles can be synthesized for various biomedical applications.[30–32]

In recent years, considerable efforts have been devoted to anchor metal particles on the framework of CNTs for their biomedical applications[9, 26] In particular, decoration of CNTs with noble metal nanoparticles is an intriguing subject because of the attractive properties of noble metal nanoparticles. Amongst the noble metals, silver nanoparticles have attracted special attention for their advantage in various studies, such as photosensitive components, electrocatalysis, chemical sensors, catalysis, and optical devices.[33–34] Silver nanoparticles deposited on inert and conducting materials appear to be good electrocatalysts for the oxidation of organic molecules.[34] Overall, silver nanoparticles are well known for their antimicrobial activity against bacterial pathogens.[35–36] In view of present desires, the hybrid materials comprised of CNTs, dendrimers and silver nanoparticles could emerge with range of interesting properties.

In this paper, we described the supramolecular functionalization of multiwalled carbon nanotubes (MWCNTs) with *p*-phenylenediamine and methylmethacrylate. The MWCNTs were functionalized with *p*-phenylenediamine through amide linkage, and subsequently with methylmethacrylate following the Michael addition. Fourth generation (G4) amine terminated dendrimers were covalently attached to acid treated MWCNTs (MWCNTs-COOH). Afterwards the Ag nanoparticles were embedded on functionalized MWCNTs (*f*-MWCNTs) by dispersing them in an aqueous solution of $AgNO_3$, without any additional reducing agent. The structure and nature of *f*-MWCNTs and *f*-MWCNTs-Ag nanohybrids were characterized by UV-vis spectroscopy, Fourier transform infrared spectroscopy (FTIR), Raman spectroscopy, powder X-ray diffraction (XRD), scanning electron microscopy (SEM) transmission electron microscopy (TEM), X-ray energy dispersive spectroscopy (EDS) and thermogravimetric analysis (TGA). The antimicrobial activity of carboxylated MWCNTs (MWCNTs-COOH), amino-functionalized MWCNTs (*f*-MWCNTs) and Ag nanoparticles decorated functionalized MWCNTs (*f*-MWCNTs-Ag) were comparatively studied against different pathogens.

2. EXPERIMENTAL DETAILS

2.1. Materials

MWCNTs prepared by chemical vapor deposition (CVD) were obtained from Carbon Nanotechnology Laboratory at Rice University, Houston TX, USA. The sulfuric acid, nitric acid and methanol were purchased from Fischer. Toluene, thionyl chloride, *p*-phenylenediamine, tetrahydrofuran, methylmethacrylate and silver nitrate were obtained from Sigma-Aldrich and were used as received. All aqueous solutions were prepared with ultrapure water obtained from the Milli-Q Plus system (Millipore).

2.2. Functionalization of MWCNTs

Pristine MWCNTs were refluxed under stirring in 1:3 (v/v) HNO_3 and H_2SO_4 at 70 °C for 24 h. Then the mixture was filtered through 0.22 μm Millipore polycarbonate membrane and several time washed with DI water until the pH reaches the range from 4 to 7. Thus prepared carboxylated MWCNTs (MWCNTs-COOH) was dried under vacuum at 40 °C for 24 h and further reacted with excess of $SOCl_2$ at room temperature for 24 h. The resulting acylated MWCNTs (MWCNTs-COCl) was separated by filteration, washed with anhydrous tetrahydrofuran and dried in vacuum at 40 °C for 12 h. After that, MWCNTs-COCl was dispersed in tetrahydrofuran by sonication for 25 min and the excess of *p*-phenylenediamine was added. This mixture was stirred at 60 °C for 12 h, filtered and washed with anhydrous tetrahydrofuran. The product, MWCNTs-NH_2 thus synthesized was delete dried overnight at 40 °C. Then the dendrimer functionalized MWCNTs (*f*-MWCNTs) were achieved by repeating the Michael addition of methylmethacrylate to the surface amino groups and amidation of terminal ester groups with *p*-phenylenediamine. The covalent functionalization of MWCNTs is illustrated in Scheme 1.

2.3. Preparation of *f*-MWCNTs and Silver Nanoparticles Hybrids

Aromatic polyamide functionalized MWCNTs (*f*-MWCNTs, 100 mg) were dispersed in 15 mL DI water by sonication for 25 min. An amount of 10 mL aqueous solution of $AgNO_3$ (0.01 mol · L^{-1}) was added drop wise to aqueous solution of dispersed *f*-MWCNTs. The mixture was stirred under ambient conditions for 8 h. The resulting *f*-MWCNTs-Ag nanohybrids were centrifuged and subsequently washed with DI water to remove any loosely adsorbed nanoparticles. The *f*-MWCNTs-Ag nanohybrids thus obtained were dried in vacuum at 40 °C for 12 h and used for further characterization. The synthetic procedure followed in the preparation of *f*-MWCNTs-Ag nanohybrids is schematically depicted in Scheme 2.

2.4. Estimation of Antimicrobial Activity

The antibacterial activity of MWCNTs-COOH, *f*-MWCNTs and *f*-MWCNTs-Ag nanohybrids were tested at Hygeia Laboratories Inc. Houston, TX, USA. The tests were performed against the Gram-positive bacterium, *Staphylococcus aureu (S. aureu)* and the Gram-negative bacteria, *Escherichia coli (E. coli)* and *Pseudomonas aeruginosa (P. aeruginosa)*. All the microorganisms were subcultured on Trypticase Soy Agar for 24 h and washed with phosphate buffered saline (PBS). The samples were diluted in PBS to provide a concentration of 20 μg/mL for the tests. An amount of 20 μL of the bacterial suspension in USP phosphate buffer (pH 7.2) was transferred to 1 mL of the prepared sample (11 μg MWCNTs-COOH/mL, 20 μg *f*-MWCNTs/mL, or 20 μg *f*-MWCNTs-Ag nanohybrid/mL) in a test tube. The inoculated samples were kept in an incubator at 37 °C for 1 h with vortexing at every 15 min. After incubation, 1 mL of the sample was transferred to 9 mL of neutralizing broth and the mixture was left to stand in room temperature for 15 min. Then the tube was vortexed, and a series of 10-fold dilutions in neutralizing broth were prepared

and plated out in Trypticase Soy Agar. The plates were incubated at 37 °C for 24 h and recorded the colony forming units (CFU). All the tests were performed in triplicate to ensure reproducibility and the percentage of microbe reduction (%R) was calculated using the equation,

$$\%R = (C_c - C_s / C_c) \times 100$$

where C_C (CFU) is the number of microbial colonies recorded on control and C_S (CFU) is the number of microbial colonies recorded on sample.

2.5. Characterization

UV-vis absorption spectra were recorded on a Varian Carry 50 Bio UV-vis spectrophotometer. FTIR spectra were recorded using a Thermo-Nicolet IR 2000 spectrometer (KBr pellet). Thermogravimetric analyses were performed with a Perkin Elmer Diamond TG/DTA instrument at a heating rate of 10 °C/min under flow of nitrogen. Raman spectra were recorded using a Raman Systems R-3000QE system at room temperature in the back scattering configuration using an Argon ion laser with wavelength 785 nm. XRD patterns were recorded at the rate of 3°/min on a Scintag X-ray diffractometer, model PAD X, equipped with a Cu Kα photon source (45 kV, 40 mA). SEM measurements were carried out on a JEOL JXA-8900 scanning electron microscope. EDS measurements were made with a ThermoNoran EDS System 6, which was attached to JEOL JXA-8900 scanning electron microscope. TEM measurements were performed using a Hitachi H-8100 microscope at 200 kV.

3. RESULTS AND DISCUSSION

The UV–vis spectra of pristine MWCNTs, *f*-MWCNTs and *f*-MWCNTs-Ag nanohybrids are shown in Figure 1. Pristine MWCNTs (Fig. 1(a)) displayed an absorption band at 248 nm with decreasing absorptivity, which is typical for MWCNTs.37 After dendrimer functionalization of MWCNTs, the characteristic band in *f*-MWCNTs appeared at 262 nm (Fig. 1(b)), this observed red shift in the characteristic band of MWCNTs indicates the existence of functionalized dendrimer macromolecules on the surface of MWCNTs. The spectrum of *f*-MWCNTs-Ag nanohybrids (Fig. 1(c)) has displayed two characteristic bands related to the presence of *f*-MWCNTs and Ag nanoparticles. The band at 266 nm is attributed to *f*-MWCNTs and the band at 370 nm is owing to surface plasmon excitation of Ag nanoparticles.

FTIR spectra of *f*-MWCNTs and *f*-MWCNTs-Ag nanohybrids were obtained to confirm the proposed structural rearrangement on the surface of MWCNTs and are shown in Figure 2. The spectrum of *f*-MWCNTs (Fig. 2(a)) displayed an absorption band at 3427 cm^{-1} which is attributed to N–H stretching frequency. The bands at 2851 and 2922 cm^{-1} are assigned to symmetric and asymmetric stretching of $–CH_2$. The band appeared at 1621 cm^{-1} was due to the carbonyl stretching of amide (–CO–NH). The presence of the band at 1031 cm^{-1} is another characteristic signal from –CO–NH absorption. In addition, the bands for the presence of aromatic ring are observed at 1515 cm^{-1} (aromatic C–C), 1031 and 1113 cm^{-1} (–CH) and 826 cm^{-1} (C–H para-aromatic out of plane vibration).38 The spectum of *f*-MWCNTs-Ag nanohybrids (Fig. 2(b)) displayed all the bands present in *f*-MWCNTs (Fig. 2(a)), the most obvious changes observed are in their band position. In Figure 2(b), the N–H stretching was observed at 3341 cm^{-1}, where as symmetric and asymmetric stretching of $–CH_2$ was observed at 2855 and 2924 cm^{-1}. The characteristic band from –CO–NH was displayed at 1605 cm^{-1} and the bands from aromatic ring are observed at 1509 cm^{-1} (aromatic C–C), 1016 and 1162 cm^{-1} (–CH) and 831 cm^{-1} (C–H para-aromatic out of plane

vibration). The conformational changes observed by shifting of bands in *f*-MWCNTs-Ag nanohybrids indicate the formation of stable nanohybdrids by the deposition of silver nanoparticles on the surface of *f*-MWCNTs.

The crystalline structure of modified MWCNTs was assessed by XRD analysis. Figure 3 depicts the XRD patterns of pristine MWCNTs, *f*-MWCNTs and *f*-MWCNTs-Ag nanohybrids. The diffraction peaks with 2θ value of 25.56° and 43.45° for pristine MWCNTs (Fig. 3(a)) and the peaks at 25.54° and 43.75° for *f*-MWCNTs (Fig. 3(b)) are corresponds to (002) and (110) reflections of graphite from the MWCNTs.39 The shifting of characteristic peak position in the XRD pattern of *f*-MWCNTs shows the perfect modification of pristine MWCNTs. There is no drastic change in the position of characteristic peaks of pristine MWCNTs and *f*-MWCNTs was observed, which suggest that MWCNTs are well retained their original structure after functionalization also. Figure 3(c) is the XRD pattern of *f*-MWCNTs-Ag nanohybrids, the diffraction peaks at 38.03°, 44.24° and 64.26° can be readily indexed to (111), (200) and (220) Bragg's reflections of silver with face centered cubic (fcc) symmetry.26, 40 This demonstrates the deposition of Ag nanoparticles in their metallic state on the surface of *f*-MWCNTs. The characteristic diffraction peaks of MWCNTs are not clearly visible in *f*-MWCNTs-Ag nanohybrids due to high intense peaks generated from strongly attached Ag nanoparticles to the surface of aromatic polyamide functionalized MWCNTs (*f*-MWCNTs). The estimated domain size of silver nanoparticles using (111) reflection by the Scherrer equation41 is ca. 35 nm.

The Raman spectra of MWCNTs-COOH, *f*-MWCNTs and *f*-MWCNTs-Ag nanohybrids obtained with an excitation of 785 nm laser is shown in Figure 4. All the spectra displayed the D- and G-bands around 1270 and 1570 cm^{-1}, respectively, corresponding to disorder and tangential modes of MWCNTs. Furthermore, the spectra of MWNT-COOH and *f*-MWCNTs exhibited the D_2-band at 1650 cm^{-1}, which is known to be directly affected by the disorder in nanotubes. In all the spectra, G-band is barely detectable against the noise. There is no significant shifts of bands were observed when the MWCNTs-COOH is functionalized with dendrimer molecules and further with Ag nanoparticles. The absolute intensity of disorder (D) mode band in the spectrum of *f*-MWCNTs (Fig. 4(b)) is higher than the intensity in the spectrum of MWNT-COOH (Fig. 4(a)). This increase in the intensity of D-band corresponds to conversion of hybridization of C atoms on the nanotubes from sp^2 to sp^3, which indicates covalent functionalization of MWNT-COOH. The spectrum of *f*-MWCNTs-Ag nanohybrids (Fig. 4(c)) has displayed the broadened D- and G-bands, in addition the D_2-band is not present, these conformational changes might arise from the deposition of Ag nanoparticles on the surface of *f*-MWCNTs.

In order to investigate the degree of functionalization of MWCNTs, thermogravimetric analyses were conducted and the thermograms obtained are shown in Figure 5. There is no significant weight loss was observed for carboxylated MWCNTs (MWCNTs-COOH) (Fig. 5(a)) up to 600 °C (11.4%). Whereas at the same temperature, generation 2, (*f*-MWCNTs/G2) (Fig. 5(b)), generation 3 (*f*-MWCNTs/G3) (Fig. 5(c)) and generation 4 (*f*-MWCNTs/G4, i.e., *f*-MWCNTs) (Fig. 5(d)) show 29.3, 49.3 and 62.1% weight loss, respectively, which is ascribed to the presence of aromatic polyamide dendrimer, grafted on the surface of MWCNTs. The thermal degradation of functionalized MWCNTs (Figs. 5(b–e)) consist of two weight loss steps due to different functional groups present on the surface of *f*-MWCNTs. The first weight loss below 300 °C could be ascribed to partial decomposition of covalently bonded dendrimers and the second weight loss could be attributed to the thermal decomposition of the defect sites of MWCNTs. The single inflection in the weight loss up to 300 °C indicates the presence of covalently bonded aromatic polyamide dendrimers on the surface of MWCNTs. The presence of organic contents on the surface of MWCNTs is estimated from the residual weight remained at 800 °C, which is 42.2%, 53.4% and 64.8%

for generation 2, 3 and 4, respectively. The thermal degradation of *f*-MWCNTs-Ag nanohybrids (Fig. 5(e)) is different from *f*-MWCNTs/G4 i.e., *f*-MWCNTs (Fig. 5(d)) and the residual weight remained at 800 °C is 39.9%, which indicates the incorporated silver nanoparticles in *f*-MWCNTs-Ag nanohybrids are stable and strongly bonded.

The SEM image of *f*-MWCNTs-Ag nanohybrids is shown in Figure 6(a), which demonstrates that *f*-MWCNTs bundles are more dissociated and less tightly bound with each other in *f*-MWCNTs-Ag nanohybrids, which would lead to the enhancement in solubility. The best spatial resolution was insufficient to clearly identify the presence of silver nanoparticles in Figure 6(a), this task was accomplished by TEM analysis. The TEM images shown in Figures 6(b–d) display the morphology of *f*-MWCNTs after deposition of Ag nanoparticles. It could be observed in Figure 6(b) that the *f*-MWCNTs bundles are separated and distributed homogeneously in *f*-MWCNTs-Ag nanohybrids, which suggests the uniform attachment of dendrimers on each nanotube. It can also be seen that the *f*-MWCNTs are well covered with homogeneosuly distributed, uniform sized silver nanoparticles. The average size of silver nanoparticles calculated from TEM is found to be ca. 34 ± 1.2 nm, which is consistent with the particle size calculated from Scherrer equation. The presence of silver nanoparticles along the sidewalls of *f*-MWCNTs (Figs. 6(c and d)) indicates the existence of strong interaction between aromatic polyamide dendrimers and silver nanoparticles. There is no loosely bonded or free standing nanoparticle present in the void space, which demonstrates that the nanoparticles incorporated in *f*-MWCNTs-Ag nanohybrids are stable. The lower contrast of dendrimers does not allow the visualization of the anchoring of dendrimers on the surface of MWCNTs. These results indicate that the dendrimer macromolecules, covalently attached on the surface of MWCNTs-COOH play a role as platforms for the formation of Ag nanoparticles and these platforms are acting as a substrate for the nucleation of silver nanoparticles. The EDS results further reveal the presence of silver in the *f*-MWCNTs-Ag nanohybrids (Fig. 7). The C signal originates from MWCNTs, and a small part of that contributes from the surface organic molecules. The Ag signal produced from the silver nanoparticles present in the nanohybrids, whereas the Al, Si and Ti signals generated from the substrate. Thus the TEM and EDS results confirm the successful deposition of silver nanoparticles on the surface of *f*-MWCNTs.

The antibacterial activity of MWCNTs-COOH, *f*-MWCNTs and the *f*-MWCNTs-Ag nanohybrids is graphically shown in Figure 8. The MWCNTs-COOH has the microbe reduction capacity of 34.1 ± 1.9%, 26.9 ± 1.1% and 22.8 ± 1.8% for *E. coli, P. aeruginosa* and *S. aureu*, respectively. The *f*-MWCNTs showed the microbe reduction of 72.6 ± 2.6%, 65.2 ± 1.9% and 35.5 ± 2.1% for *E. coli, P. aeruginosa* and *S. aureu*, respectively. Whereas, the microbe reduction capability of the *f*-MWCNTs-Ag nanohybrids is 93.7 ± 1.5%, 69.7 ± 1.9% and 56.7 ± 1.8% for *E. coli, P. aeruginosa* and *S. aureu*, respectively. The antibacterial activity of MWCNTs-COOH is significantly enhanced by functionalizing with aromatic polyamide dendrimer (*f*-MWCNTs), which further improved by incorporation of silver nanoparticles onto *f*-MWCNTs. Thus *f*-MWCNTs and the *f*-MWCNTs-Ag nanohybrids showed stronger antimicrobial effect than MWCNTs-COOH against all the three tested bacteria. The presence of silver nanoparticles is significantly improved the antibacterial efficiency of the *f*-MWCNTs-Ag nanohybrids. Thus the antimicrobial activity of silver nanoparticles in dendrimeric matrix proved to be important for the prevention of adherence and proliferation activities of bacteria. The *f*-MWCNTs-Ag nanohybrids showed higher antibacterial activity against Gram-negative bacteria, *E. coli* and *P. aeruginosa* compared with Gram-positive bacterium, *S. aureu*. This observed variation in the activity of Gram-positive and Gram-negative bacteria might be due to difference in their membrane structure. The most distinctive difference lies in the thickness of the cell wall, composed of peptidoglycan. The peptidoglycan layer of Gram-positive bacteria (about 20–80 nm) is usually thicker than that of Gram-negative bacteria (about 7–8 nm).26 The thinner cell wall

of Gram-negative bacteria results in the stronger interaction between negatively charged bacterial wall and dendrimer macromolecules, which can possibly increase the contact area between Ag nanoparticles and bacteria.42

4. CONCLUSIONS

In summary, the multiamine comprised dendritic molecular structures were successfully constructed on the surface of pristine acid treated MWCNTs by repeated polymerization of *p*-phenylenediamine and methylmethacrylate. The covalent attachment of fourth generation aromatic polyamide dendrimers on the surface of MWCNTs-COOH was achieved through Michael addition and amidation reactions. The numerous functional amine groups on the surface of *f*-MWCNTs played an important role in the *in-situ* reduction of Ag^+ ions and simultaneous formation of silver nanoparticles, under ambient conditions without any additional chemical or irradiation technique. The efficient exfoliation of *f*-MWCNTs and homogeneous distribution of Ag nanoparticles in *f*-MWCNTs-Ag nanohybrids is an indication of the effectiveness of our functionalization method. Our findings revealed that *f*-MWCNTs and *f*-MWCNTs-Ag nanohybrids have higher antibacterial activity than MWCNTs-COOH against against *E. coli, P. aeruginosa* and *S. aureu*. The antibacterial activity of pristine MWCNTs is drastically enhanced by the functionalization with hyperbranched aromatic polyamide, which further improved by the immobilization of Ag nanoparticles. The *f*-MWCNTs-Ag nanohybrids showed higher antibacterial activity against the tested Gram-negative bacteria, *E. coli* and *P. aeruginosa*. The strategy of this method is also suitable for the preparation of nanohybrids containing *f*-MWCNTs and other noble metal nanoparticles. The prepared multifunctional *f*-MWCNTs-Ag nanohybrids are stable and biocompatible, so these nanohybrids could be used as a nanoplatform for the development of CNTs based antibacterial materials.

Acknowledgments

Authors acknowledge the support from NIH Grant No. 1 SC3 GM078361-01, the Welch Foundation, the US Air Force Research Laboratory Minority Leaders Nanocomposite Project and USDA Evans-Allen Fund.

References and Notes

1. Kulamarva A, Raja PMV, Bhathena J, Chen H, Talapatra S, Ajayan PM, Nalamasu O, Prakash S. Nanotechnology. 2009; 20:25612.
2. Banks CE, Moore RR, Davies TJ, Compton RG. Chem. Commun. 2004:1804.
3. Wang J. Electroanalysis. 2005; 17:7.
4. Hong SY, Tobias G, Al-Jamal KT, Ballesteros B, Ali-Boucetta H, Lozano-Perez S, Nellist PD, Sim RB, Finucane C, Mather SJ, Green MLH, Kostarelos K, Davis BG. Nat. Mater. 2010; 9:485. [PubMed: 20473287]
5. Heister E, Neves V, Tilmaciu C, Lipert K, Beltran VS, Coley HM, Silva SRP, McFadden J. Carbon. 2009; 47:2152.
6. Chen J, Hamon MA, Hu H, Chen YS, Rao AM, Eklund PC, Haddon RC. Science. 1998; 282:95. [PubMed: 9756485]
7. Jimeno A, Goyanes S, Eceiza A, Kortaberria G, Mondragon I, Corcuera MA. J. Nanosci. Nanotechnol. 2009; 9:6222. [PubMed: 19908518]
8. Oki A, Adams L, Luo Z, Osayamen E, Biney P, Khabashesku V. J. Phys. Chem. Solids. 2008; 69:1194. [PubMed: 18548126]
9. Tao L, Chen GJ, Mantovani G, York S, Haddleton DM. Chem. Commun. 2006:4949.
10. Zhang Q, Naito K, Kagawa Y. J. Nanosci. Nanotechnol. 2009; 9:267. [PubMed: 19441306]
11. Oki A, Adams L, Luo Z. Inorg. Chem. Commun. 2008; 11:275.

12. Simmons TJ, Bult J, Hashim DP, Linhardt RJ, Ajayan PM. ACS Nano. 2009; 3:865. [PubMed: 19334688]
13. Lee SS, Lee DS. J. Nanosci. Nanotechnol. 2010; 10:3370. [PubMed: 20358959]
14. Song L, Qiu Z. J. Nanosci. Nanotechnol. 2010; 10:965. [PubMed: 20352743]
15. Morishita T, Matsushita M, Katagiri Y, Fukumori K. Carbon. 2010; 48:2308.
16. Dalton AB, Stephan C, Coleman JN, McCarthy B, Ajayan PM, Lefrant S. J. Phys. Chem. B. 2000; 104:10012.
17. Chen RJ, Zhang Y, Wang D, Dai H. J. Am. Chem. Soc. 2001; 123:3838. [PubMed: 11457124]
18. Star A, Stoddart JF, Steuerman D, Diehl M, Boukai A, Wong EW. Angew. Chem. Int. Ed. 2001; 40:1721.
19. Chen J, Liu H, Weimer WA, Halls MD, Waldeck DH, Walker GC. J. Am. Chem. Soc. 2002; 124:9034. [PubMed: 12148991]
20. Carson L, Kelly-Brown C, Stewart M, Oki A, Regisford G, Luo Z, Bakhmutov VI. Mater. Lett. 2009; 63:617. [PubMed: 20200591]
21. Shen M, Wang SH, Shi X, Chen X, Huang Q, Petersen EJ, Pinto RA, Baker JR, Weber WJ. J. Phys. Chem. C. 2009; 113:3150.
22. Yang W, Thordarson P, Gooding JJ, Ringer P, Braet F. Nanotechnology. 2007; 18:412001.
23. Cui D, Ozkan CS, Ravindran S, Kong Y, Gao H. Mech. Chem. Biosyst. 2004; 1:113. [PubMed: 16783937]
24. Trollsaas M, Hedrick JL. J. Am. Chem. Soc. 1998; 120:4644.
25. Pan B, Cui D, Gao F, He R. Nanotechnology. 2006; 17:2483. [PubMed: 21727493]
26. Yuan W, Jiang G, Che J, Qi X, Xu R, Chang MW, Chen Y, Lim SY, Dai J, Chan-Park MB. J. Phys. Chem. C. 2008; 112:18754.
27. Kukowska-Latallo JF, Candido KA, Cao Z, Nigavekar SS, Majoros IJ, Thomas TP, Balogh LP, Khan MK, Baker JR. Cancer Res. 2005; 65:5317. [PubMed: 15958579]
28. Majoros IJ, Myc A, Thomas T, Mehta CB, Baker JR. Biomacromolecules. 2006; 7:572. [PubMed: 16471932]
29. Shukla R, Thomas TP, Peters JL, Desai AM, Kukowska-Latallo J, Patri AK, Kotlyar A, Baker JR. Bioconjugate Chem. 2006; 17:1109.
30. Shi X, Wang S, Meshinchi S, Van Antwerp M, Bi X, Lee I, Baker JR. Small. 2007; 3:1245. [PubMed: 17523182]
31. Lesniak W, Bielinska AU, Sun K, Janczak KW, Shi X, Baker JR, Balogh LP. Nano Lett. 2005; 5:2123. [PubMed: 16277438]
32. Shi X, Wang SH, Swanson SD, Ge S, Cao Z, Van Antwerp ME, Landmark KJ, Baker JR. Adv. Mater. 2008; 20:1671.
33. Zamudio A, Elias AL, Rodriguez-Manzo JA, Lopez-Urias F, Rodriguez-Gattorno G, Lupo F, Ruhle M, Smith DJ, Terrones H, Diaz D, Terrones M. Small. 2006; 2:346. [PubMed: 17193047]
34. Dekanski A, Stevanovic J, Stevanovic R, Jovanovic VM. Carbon. 2001; 39:1207.
35. Kumar A, Vemula PK, Ajayan PM, John G. Nat. Mater. 2008; 7:236. [PubMed: 18204453]
36. Liong M, France B, Bradley KA, Zink JI. Adv. Mater. 2009; 21:1684.
37. Shi X, Wang SH, Shen M, Antwerp ME, Chen X, Li C, Petersen EJ, Huang Q, Weber WJ, Baker JR. Biomacromolecules. 2009; 10:1744. [PubMed: 19459647]
38. Sun Z, Zhang X, Liang Y, Li H. Electrochem. Commun. 2009; 11:557.
39. Yan D, Wang F, Zhao Y, Liu J, Wang J, Zhang L, Park KC, Endo M. Mater. Lett. 2009; 63:171.
40. Neelgund GM, Hrehorova E, Joyce M, Bliznyuk V. Polym. Int. 2008; 57:1083.
41. Cullity, BD. Elements of X-Ray Diffraction. Edison-Wesley Publishing Company Inc.; 1978.
42. Sharma VK, Ria A, Yngard YL. Adv. Colloid Interface Sci. 2009; 145:83. [PubMed: 18945421]

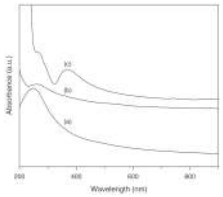

Fig. 1.
UV-vis spectra of (a) pristine MWCNTs, (b) *f*-MWCNTs and (c) *f*-MWCNTs-Ag nanohybrids.

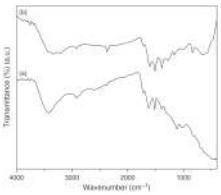

Fig. 2.
FTIR spectra of (a) *f*-MWCNTs and (b) *f*-MWCNTs-Ag nanohybrids.

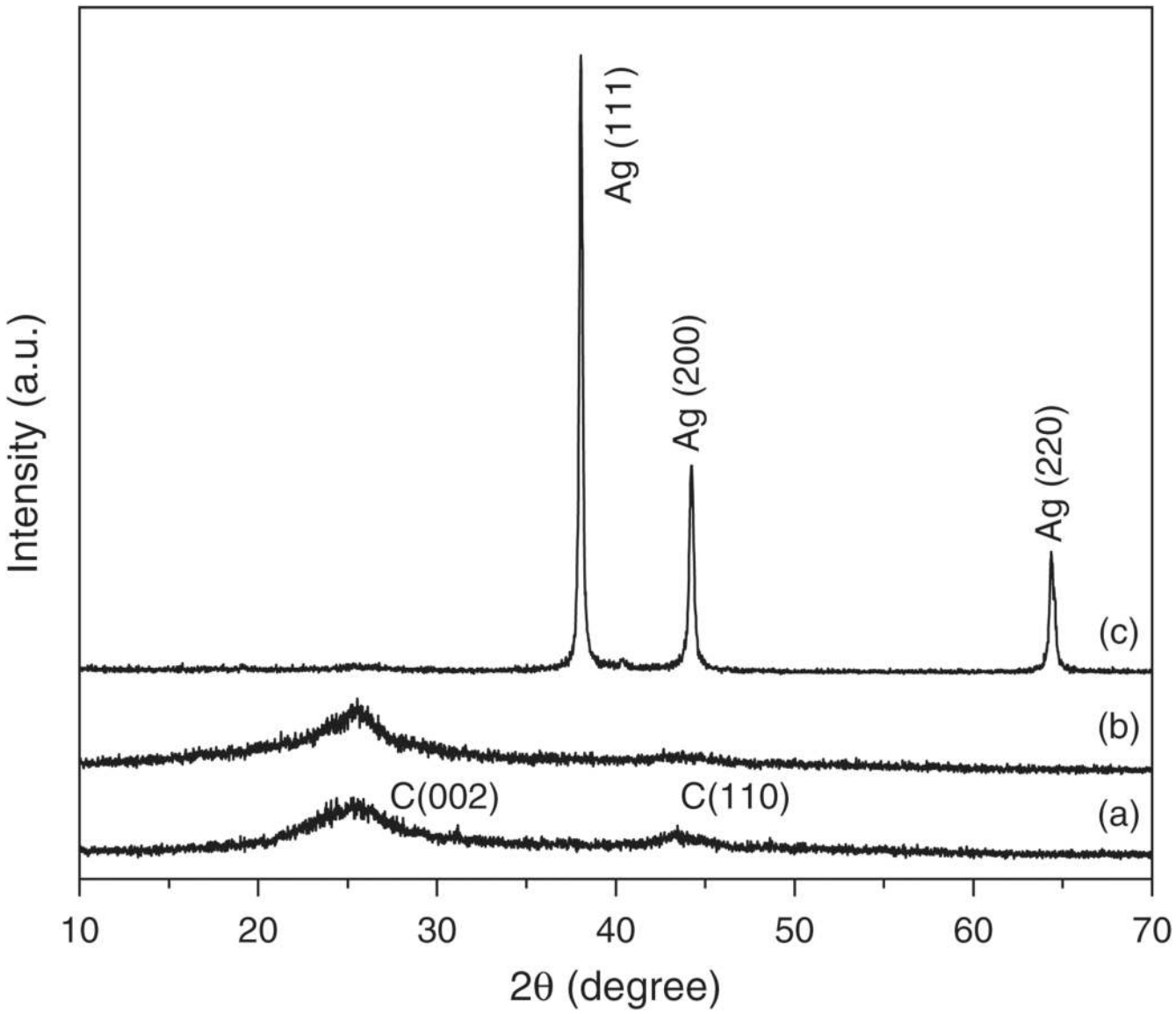

Fig. 3.
XRD patterns of (a) pristine MWCNTs, (b) *f*-MWCNTs and (c) *f*-MWCNTs-Ag nanohybrids.

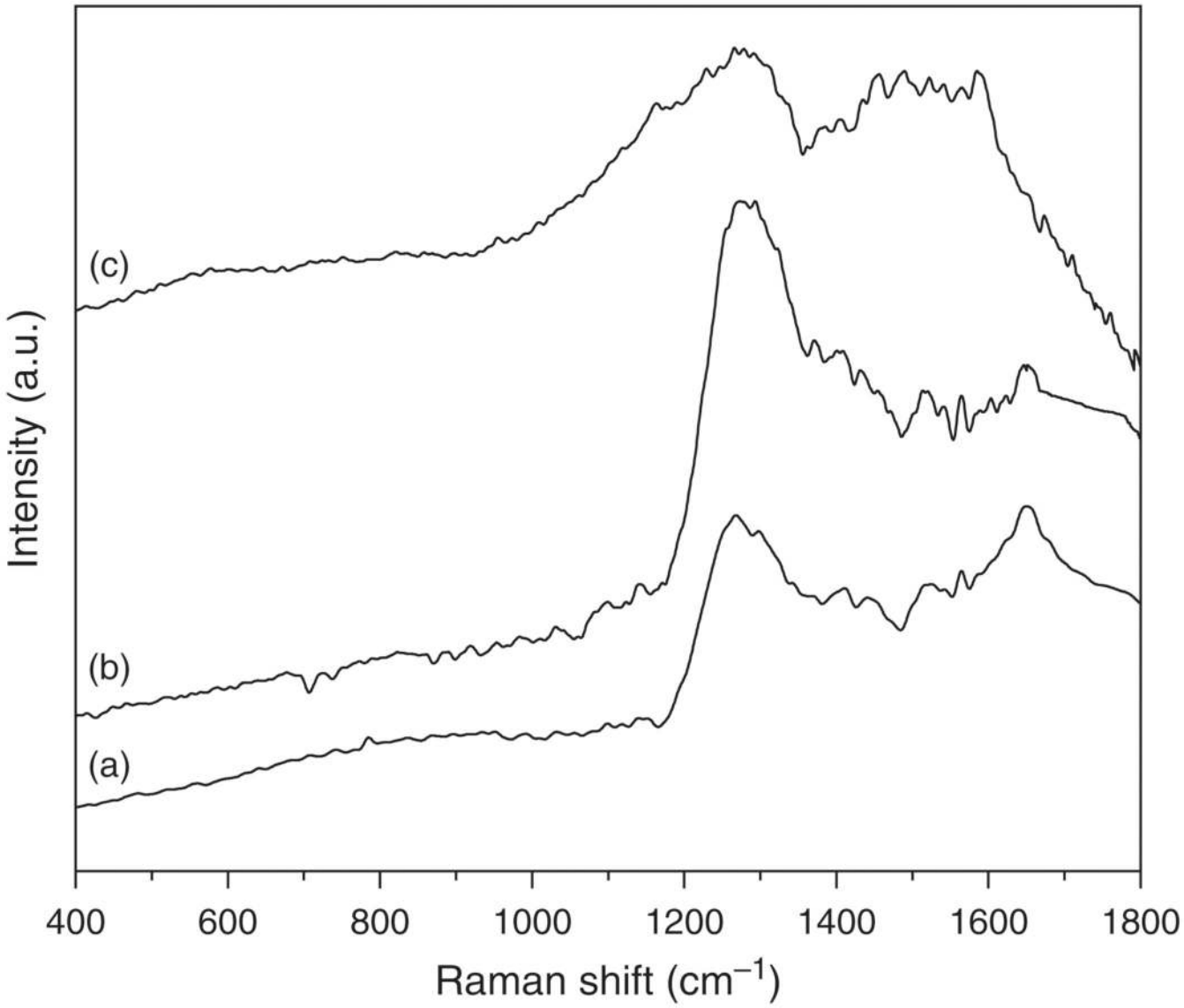

Fig. 4.
Raman spectra of (a) MWCNTs-COOH, (b) *f*-MWCNTs and (c) *f*-MWCNTs-Ag nanohybrids.

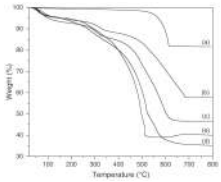

Fig. 5.
TGA thermograms of (a) MWCNTs-COOH, (b) *f*-MWCNTs/G2, (c) *f*-MWCNTs/G3, (d) *f*-MWCNTs/G4 i.e., *f*-MWCNTs and (e) *f*-MWCNTs-Ag nanohybrids.

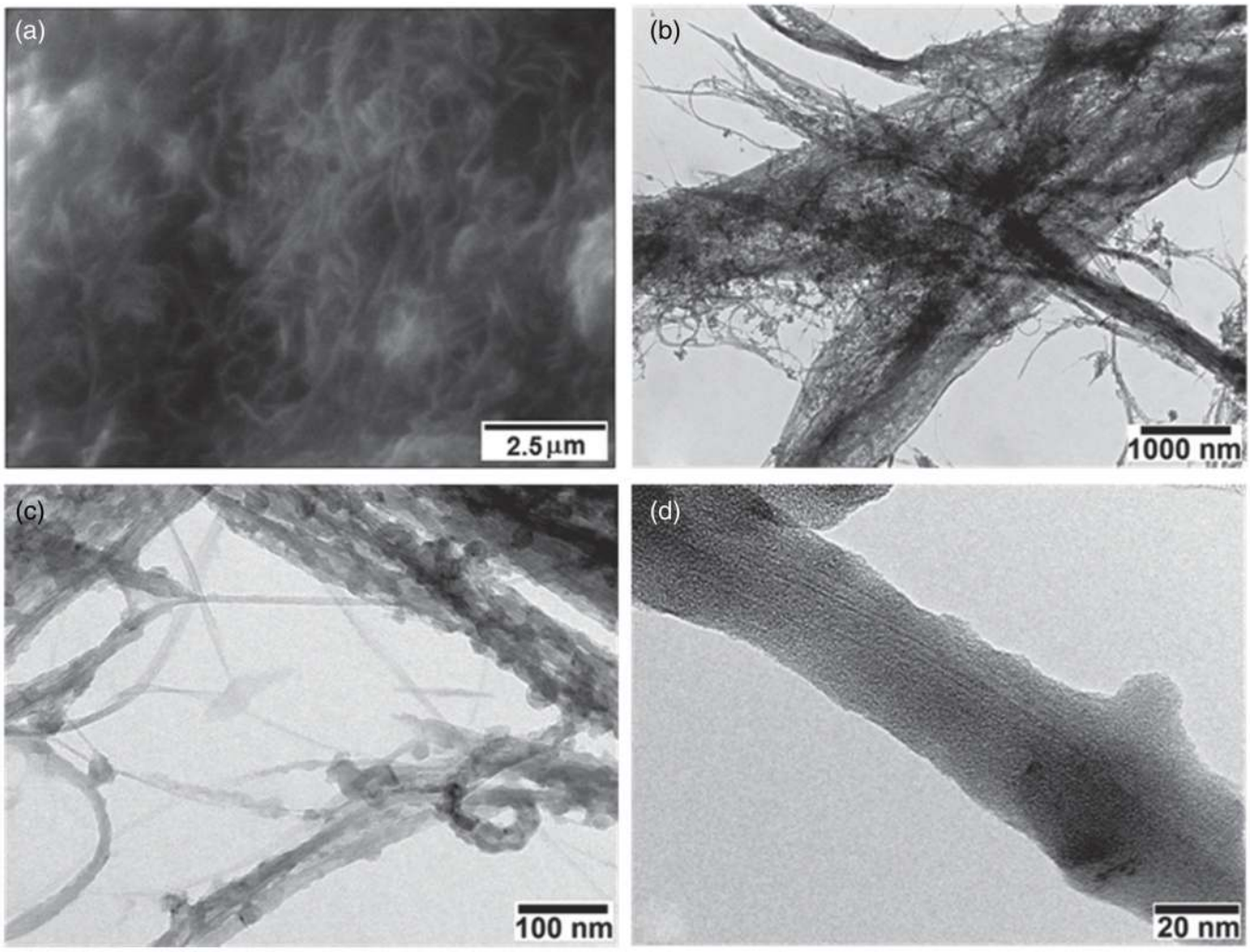

Fig. 6.
(a) SEM image and (b–d) TEM images of *f*-MWCNTs-Ag nanohybrids.

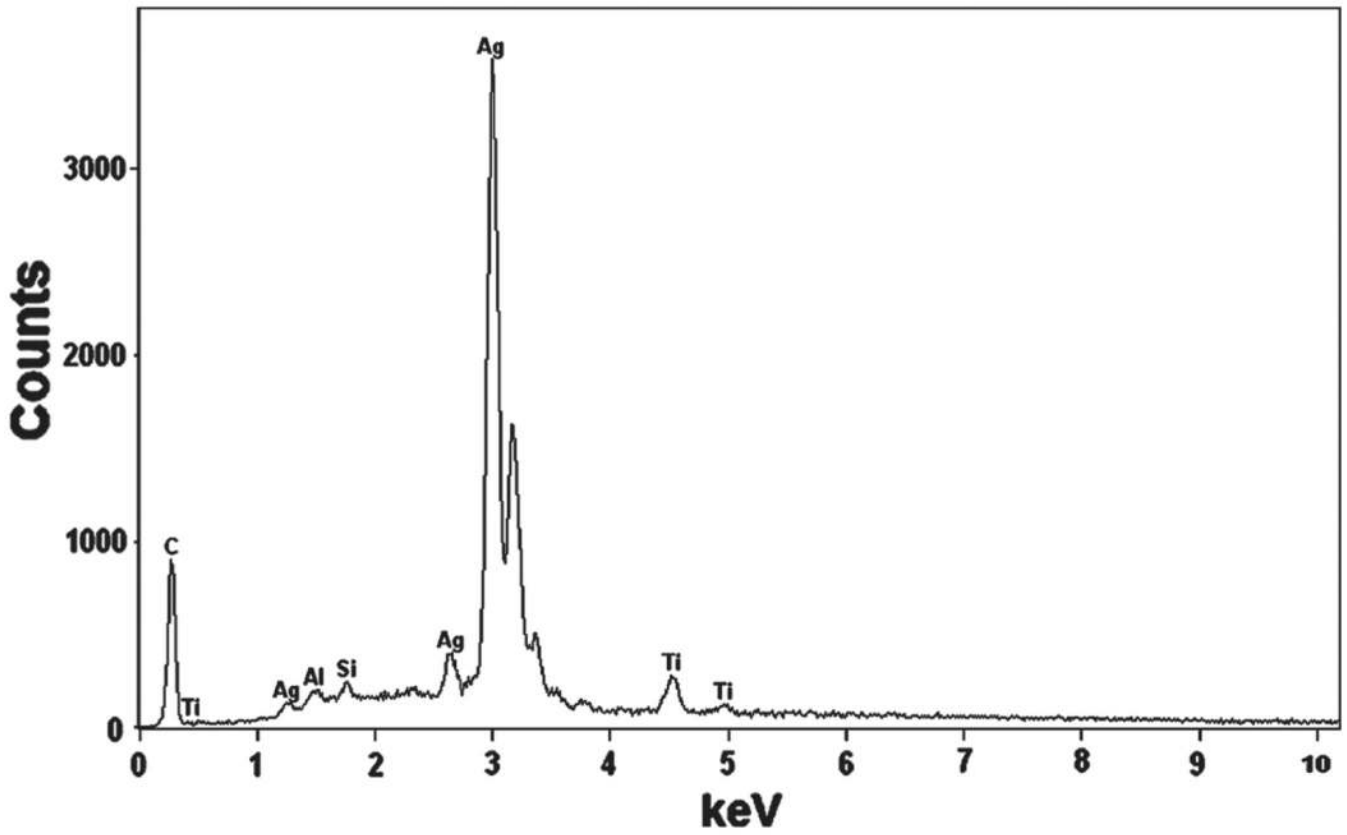

Fig. 7.
X-ray energy dispersive spectroscopy (EDS) of *f*-MWCNTs-Ag nanohybrids.

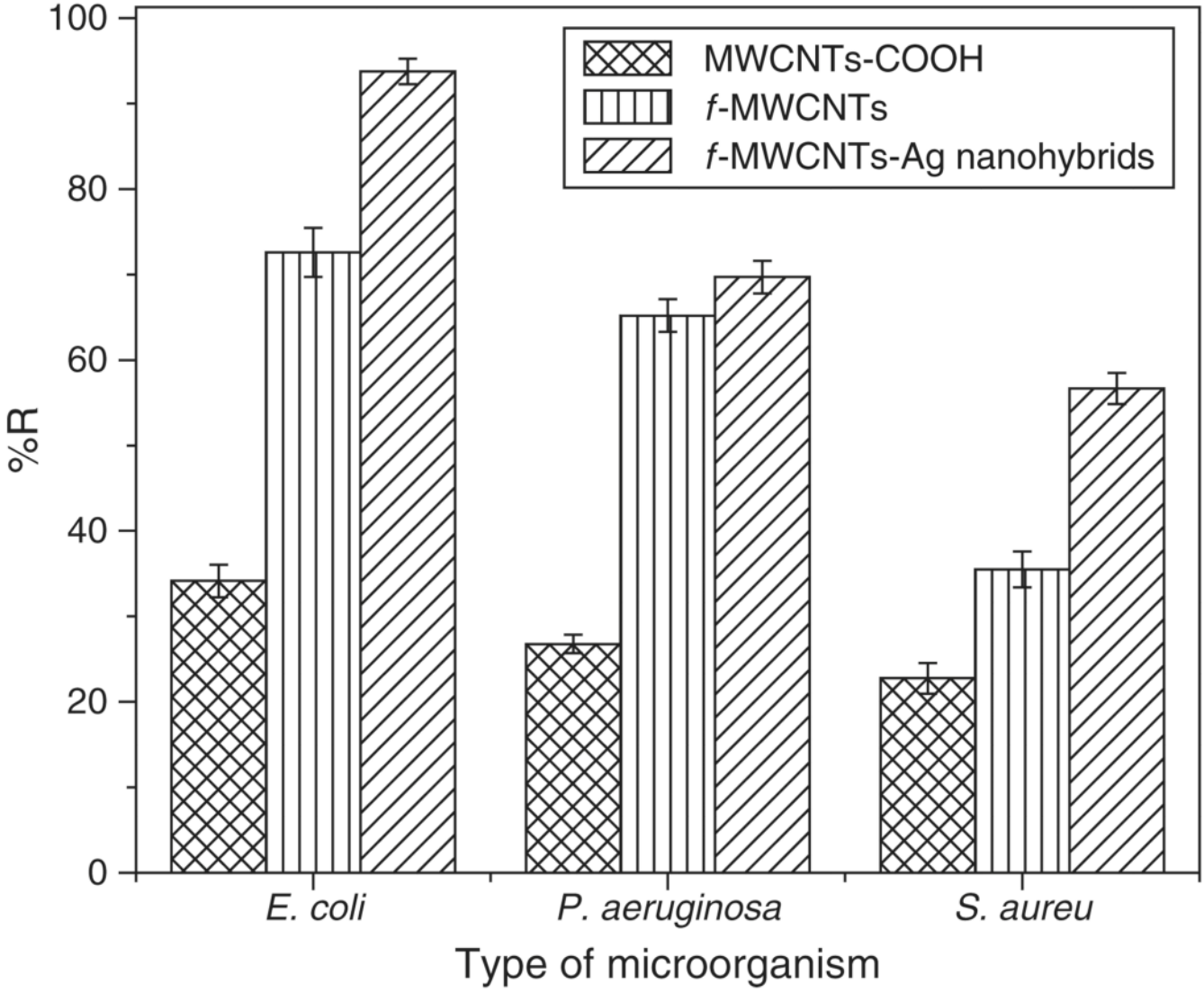

Fig. 8.
Antibacterial activity of MWCNTs-COOH, *f*-MWCNTs and the *f*-MWCNTs-Ag nanohybrids.

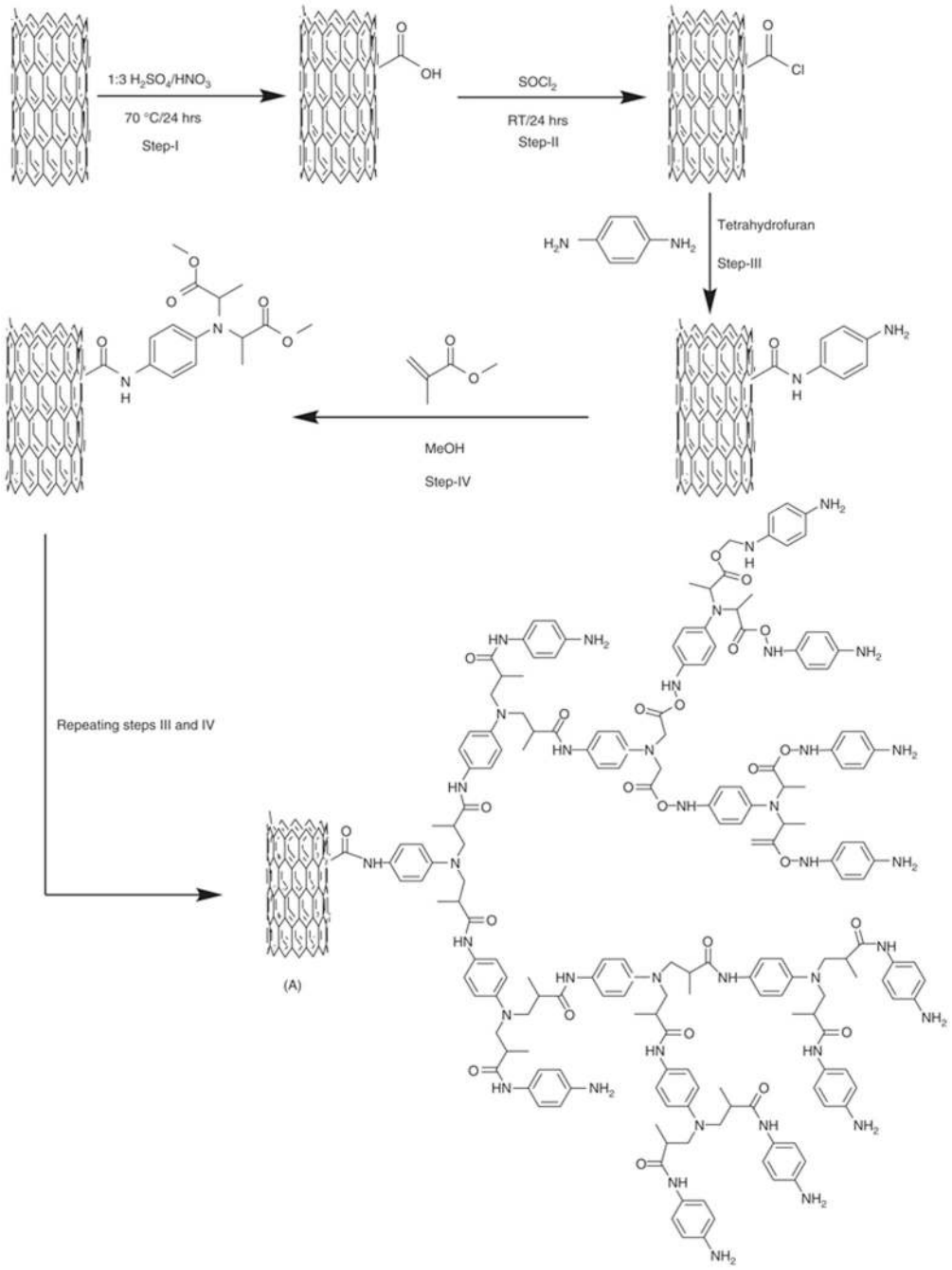

Scheme 1.
Illustration of covalent modification of pristine MWCNTs.

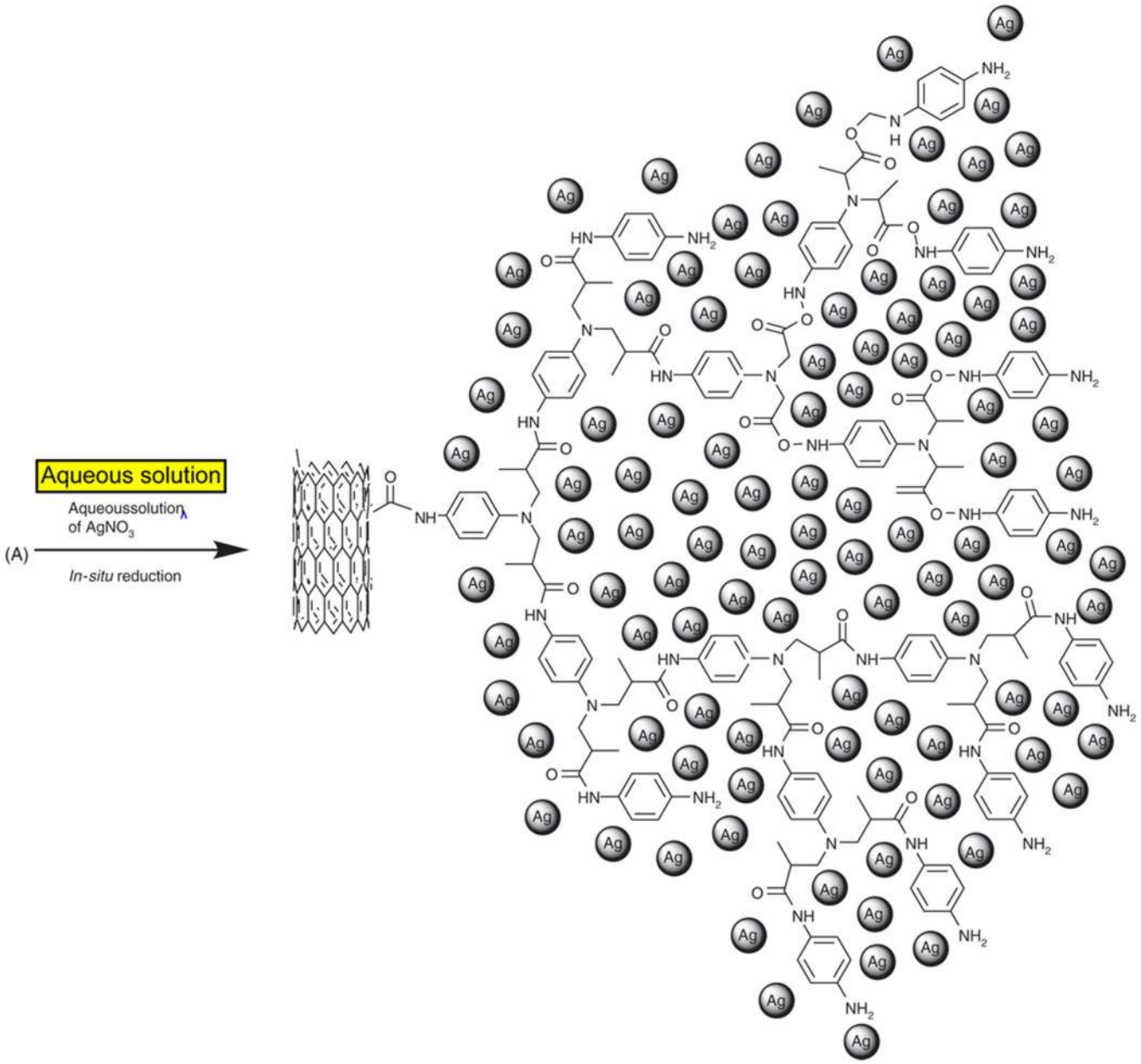

Scheme 2.
Schematic representation of *in-situ* reduction of aqueous solution of $AgNO_3$ and formation of silver nanoparticles on the surface of *f*-MWCNTs.